Original Manuscript

JOURNAL OF THERMOPLASTIC COMPOSITE MATERIALS

Determination of the anisotropic electrical conductivity of carbon fabric reinforced composites by the six-probe method

Journal of Thermoplastic Composite Materials
2023, Vol. 0(0) 1–27

DOI: 10.1177/08927057231154546
journals.sagepub.com/home/jtc
SAGE

Sebastiaan Van den Berg[1,2,3], Martin Luckabauer[2], Sebastiaan Wijskamp[1] and Remko Akkerman[1,2]

Abstract

Currently, it is challenging to obtain consistent values for the anisotropic electrical conductivity of fabric ply based thermoplastic composites. In this study, the anisotropic electrical conductivity of this type of material was obtained by combining six-probe voltage measurements with a numerical evaluation method to process the voltage measurements. The effect of probe distance and specimen dimensions on the test results was investigated. The measurements show low specimen to specimen variability and the obtained electrical conductivities agree with values obtained by the rule of mixtures and the two-probe measurement method. The conducted research shows that with one experiment, both the in- and the out-of-plane electrical conductivity of polymer composites reinforced with carbon fabrics can be reliably determined, simultaneously.

Keywords

Carbon fabric reinforced composite, electrical conductivity, anisotropy, characterisation

[1]Production Technology, University of Twente, Enschede, The Netherlands
[2]Thermo Plastic Composites Research Center, Enschede, The Netherlands
[3]GKN-Fokker Aerostructures, Hoogeveen, The Netherlands

Corresponding author:
Sebastiaan van den Berg, Production Technology, University of Twente, Drienerlolaan 5, Enschede 7500 AE, The Netherlands.
Email: s.vandenberg-1@utwente.nl

Introduction

Background

Carbon fibre reinforced polymer materials, referred to as composites, are more and more being applied in aerospace. The increasing demand for aircraft[1] drives the need for cost-efficient, high-rate production of composite structures. The last two decades have seen a growing trend towards the application of thermoplastic polymers as matrix material[2] owing to their short processing times, higher toughness and long shelf life. Since large composite structures are typically assembled from smaller components, joining techniques for composites have become a relevant research topic.

Mechanical fastening, a matured joining technology,[3] introduces problems for composites since the load carrying fibres are damaged and stress concentrations arise in the vicinity of the fasteners. Design rules have been developed to take these stress concentrations into account, unfortunately these design rules result in weight gains.[3] Adhesively bonded joints require no drilling operations and therefore, generally, weigh less compared to their fastened counter parts while creating a strong joint since stresses are distributed over large areas. However, to realise an acceptable final joint quality proper surface pretreatment is critical[3] and adhesive bonding is challenging for thermoplastic composites (TPC) due to the low surface energy of the thermoplastic polymer.

The use of a TPC enables joining separate components by fusion bonding, in which heat energy is utilized to melt the faying surface resin to achieve intimate contact and polymer chain diffusion and to accomplish the bonding process. In this technique, the healing capability of TPCs is utilised and the efficiency of the welded joint can approach the bulk properties of the adherents.[3,4] A number of fusion bonding, or welding, techniques exist[5] differing in the way heat is generated. Ultrasonic welding, induction welding and resistance welding are currently being applied during the manufacturing process of commercial aerospace structures.[3,4]

With induction welding, the heat is generated as a result of energy losses of electric currents running through the electrically conductive fibres of the composite. The electric currents are induced by the change of the magnetic flux density created by an alternating electric current in a coil located in the vicinity of the composite. The existence of closed electric loops within the conductive material is a necessary condition for induction to occur. In thermoplastic composites with a carbon fibre fabric reinforcement, the specific type of composites of the present study, the fibre bundles are able to form a closed electric loop either by direct contact or by indirect contact when separated by a small amount of the dielectric polymer.

Different heating mechanisms have already been identified in earlier studies on induction heating of composites with a carbon fibre fabric reinforcement.[6,7] These mechanisms can be distinguished in i) heating by Joule losses along the fibre bundles; ii) heating by contact resistance at junctions between fibre bundles; and iii) heating by dielectric hysteresis at the fibre bundle junctions where fibres are separated by a layer of thermoplastic polymer.[6,8–10] These three mechanisms are depicted in Figure 1. The amount in which each mechanism contributes to the total heat generation depends on the

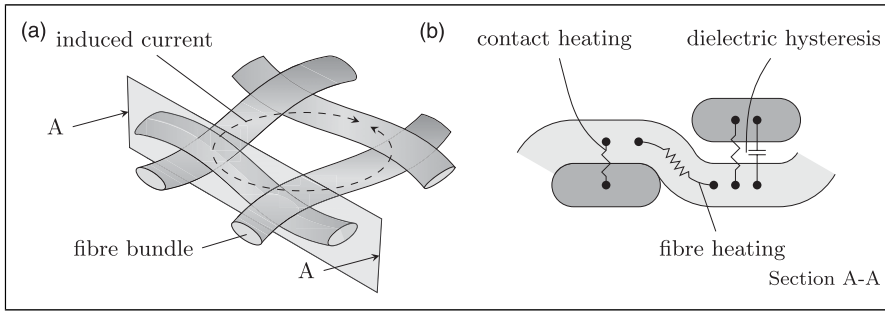

Figure 1. Schematic overview of the heating mechanisms in induction heating of thermoplastic composites with woven reinforcement.

electrical properties of the constituents in a ply as well as on the architecture of the fabric. Mitschang et al.[11] showed that direct fibre contacts are formed at the junctions of the interlacing fibre bundles in a fabric ply. The adjacent plies in a laminate are likely to be in direct contact, although the extent of contact is unknown.

Currently, the process window definition of an induction welding process in industrial practice in which fabric-ply based TPCs are joined,[12] largely relies on empirical methods. Once the process window is defined, high repeatability of the weld quality is obtained by proper process control. Nevertheless, insufficient fundamental understanding of the process prevents properly anticipating (and, if needed, mitigating) the effect of a change somewhere in the process chain on the weld quality. Moreover, an accurate predictive capability accelerates the specification of induction welding process parameters which is key in reducing cost and turnaround time for larger thermoplastic composite parts.

The process window could be defined using existing numerical simulation software, e.g. COMSOL Multiphysics[13] or Abaqus,[14] in which electromagnetic and thermal models are coupled. The outcome of these models is highly dependent on the input material property data, especially on the electrical conductivity matrix. Currently, reliable data on electrical conductivities are hardly available for most composite materials due to little consensus regarding a standardised method to characterise this property.

Publications in which the electrical conductivities of TPCs, with a carbon fibre fabric reinforcement, are required for induction heating simulations are using either anisotropic electrical conductivities[9,11,15–21] or an equivalent electrical conductivity.[22,23] While the former approach allows for the prediction of inductive heating of arbitrary laminate lay-ups and arbitrary coil configurations, the application of the latter approach is limited to bidirectional and isotropic structures[22,23] with an axisymmetric coil geometry[23] and a fibre volume fraction φ_f of at least 0.65[23]. In this study, preference is given to a generically applicable method, hence the equivalent conductivity method is not considered in this study.

The applied in-plane anisotropic electrical conductivities in the considered studies were determined by applying the rule of mixture, according to

Table 1. Overview of applied electrical conductivities at fabric ply level, normalised to a φ_f of 0.50, in published studies on simulation of heating by induction of composite materials with a carbon fibre fabric reinforcement.

Study	Material	Weave type	σ_1 [kS/m]	σ_3 [S/m]	Ref
Moser	T300/PPS T300/PEEK	5HS	13.9	0.0	[16]
Pappada et al	T300/PPS	5HS	—	—	[17]
Duhovic et al	T300/PEEK	5HS	13.9	0.0	[18]
Lionetto et al	T300/PEEK	5HS	4	0.3	[19]
Lundström et al	AS4/D.E.N. 425[a]	twill	15.8	6.0	[20]
Duhovic et al	CF/PA66	NCF	12.5	1.0	[21]

[a]D.E.N.™ 425Epoxy Novolac is a liquid reaction product of epichlorohydrin and phenol-formaldehyde novolac.

$$\sigma_1 = \varphi_{f,1}\sigma_f + \left(1 - \varphi_{f,1}\right)\sigma_m, \tag{1a}$$

$$\sigma_2 = \varphi_{f,2}\sigma_f + \left(1 - \varphi_{f,2}\right)\sigma_m, \tag{1b}$$

where σ represents the electrical conductivity and φ_f the fibre volume fraction. The subscripts 1 and 2 denote the warp and weft direction of the fabric and the subscripts f and m represent the fibre material and the polymer matrix, respectively. Since the polymer matrix is an electric isolator, the second part of these equations can be neglected and equation (1) reduces to

$$\sigma_1 = \varphi_{f,1}\sigma_f, \tag{2a}$$

$$\sigma_2 = \varphi_{f,2}\sigma_f. \tag{2b}$$

Lundström[20] and Duhovic[21] characterised σ_1 and the electrical conductivity in normal direction of the ply, σ_3, by combining the rule of mixtures with eddy current measurements according to the work done by Mizukami and Watanabe.[24] The other studies only applied the rule of mixtures to obtain σ_1 and assumed a negligible out-of-plane electrical conductivity since the plies in a laminate are separated by a relatively resin rich interface which, again, acts as an electric insulator. An overview of the applied σ_1 and σ_3 values at fabric ply level and at a normalised φ_f of 0.50 is summarised in Table 1 for the considered studies.

Several measurement methods are available to determine the electrical conductivity of an anisotropic material. The methods can be divided in uniform and non-uniform current density methods. Figure 2 provides a schematic overview, intended to show the basic principles of the measuring methods, of a number of methods applied in previous studies; the practical application of the electrodes to the specimens has been omitted from this schematic overview.

In most studies where the electrical conductivity of a TPC is investigated, this property is characterised by a uniform current density method. A well known uniform current

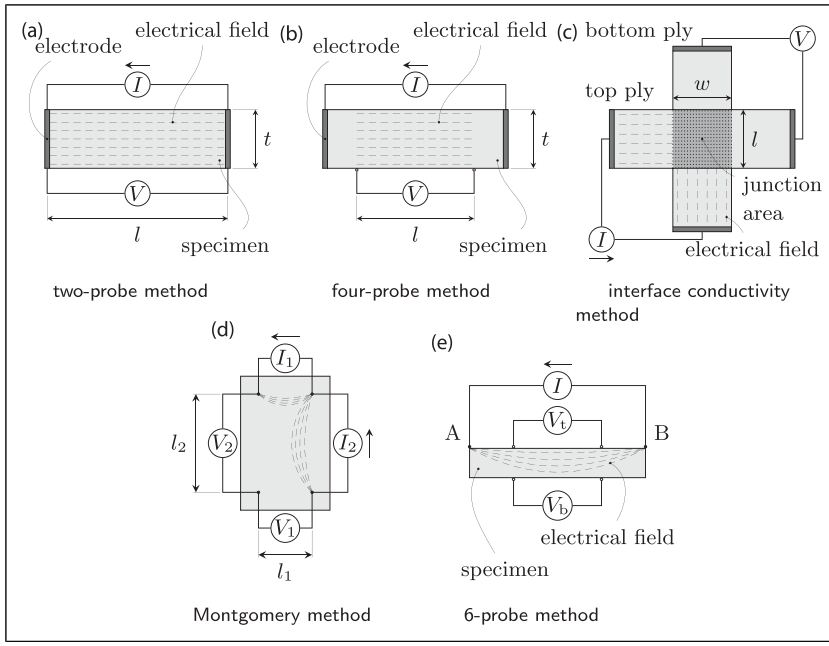

Figure 2. Schematic representation of the found electrical conductivity measurement test set-ups: (a) voltage measurements occur at contact surfaces; (b) voltage measurements using line contact probes or point contact probes; (c) voltage measurements occur at contact surfaces; (d) voltage measurements by means of point probes; (e) voltage measurements by means of line contact probes.

density method is the two-probe method of which a schematic overview is depicted in Figure 2(a). Schulte et al., Kim et al. and Todoroki et al.[7,25,26] applied this method in their studies. In this method, a direct current I is applied by electrodes which are installed at two opposing parallel end faces of the specimen. The aim is a uniform distribution of the current density across a specimen's cross-section, depicted in the figure by the equidistant dashed lines. The measured voltage drop between the electrodes, V, over distance, l, being the specimen's length, is used to calculate the conductivity by applying Ohm's law,

$$\sigma = \frac{I}{V}\frac{wt}{l} \tag{3}$$

where w and t represent the specimen's width (normal to the cross section) and thickness dimensions. The measured resistance ($R = V/I$) is a combination of the resistance in the electrode, the contact resistance between electrode and specimen and the resistance in the specimen. The electrode resistance can be assumed negligible if the electrical conductivity of the electrode material is orders of magnitude higher than the specimen's electrical conductivity. The contact resistance between electrode and specimen needs to be

minimised in order to get proper electrical conductivities of the specimen. Moreover, a high quality contact between electrode and specimen is required to generate the pursued uniform current density in the specimen. This is obtained by laborious contact surface preparation and applying sufficient clamping force between electrodes and specimen.

The four-probe method, shown in Figure 2(b), is generally applied[24,27–29] to determine a composite's in-plane electrical conductivity. Similar to the two-probe method, a direct current, I, is applied by electrodes installed at two opposing parallel end faces of the specimen. The voltage drop is measured using extra probes which are positioned between the electrodes through which the current is applied. Both point contact probes[29] as well as line contact probes[24] are used. The measurement probes eliminate the electrode resistance in the measurements. The current is assumed to be uniformly distributed between the voltage measurement probes making this method less susceptible for an inadequate contact quality between electrode and specimen and therefore the contact surface preparation might become less laborious compared to the surface preparations needed in the two-probe method. The measured voltage drop, V over distance l, is used to calculate the conductivity by applying Ohm's law, equation (3).

Wang et al.[30] and Guerrero et al.[31] investigated the electrical conductivity of the interface between the plies of a composite laminate. In their method, schematically shown in Figure 2(c) and (a) uniformly distributed current over the junction area is assumed. The interface's contact conductivity, σ_c, is calculated by,

$$\sigma_c = \frac{I}{V}\frac{1}{wl} \tag{4}$$

This method requires an evenly distributed current over the width of the electrodes to which the current is applied.

Non-uniform current density methods generally assume a specific distribution of the current density in the specimen. A well-known method to determine a material's anisotropic electrical conductivity is the so-called Montgomery method[32] and is schematically shown in Figure 2(d). The anisotropic electrical conductivities are obtained by specific voltage measurements between the point probes combined with the specimen dimensions.[32] This method is, in the case of composites, only suitable to characterise the in-plane anisotropic electrical conductivities.

In a more recent study, performed by Hart and Zhupanska,[33] the six-probe method, shown in Figure 2(e), has been investigated using uni-directional composites. In this method, an electrical current is applied through a line contact at positions A and B in the figure and voltages are measured in between these positions. The line contacts makes surface pretreatments, such as needed in the discussed uniform current density methods, superfluous. This is specifically the case when this method is applied to characterise the anisotropic electrical conductivities of carbon fabric reinforced composites, the fabric's fibre bundles oriented in the specimen's width direction take care of the distribution of the applied electrical current in this direction. However, due to the non-uniform current density distribution in the specimen's thickness direction, the determination of the

anisotropic electrical conductivities from the voltage measurements becomes more complex compared to the uniform current-density methods.

The electromagnetic eddy current measurement method is an example of another non-uniform current density method. Application of this method is reported by Mook et al.[34] and Cheng et al.[35] to be used for qualitative comparisons between composite materials rather than for quantitative purposes. More recently, Lundström et al.[20] combined rule of mixtures, equation (2), to determine σ_1, with eddy current measurements to characterise σ_3. To derive the out-of-plane electrical conductivity from the eddy current measurement data, the inverse numerical method, as described by Mizukami and Watanabe,[24] was applied.

The objective of the current research is to develop and demonstrate a reliable method to measure the anisotropic electrical conductivity of carbon fibre fabric reinforced thermoplastic composites, without being dependent on delicate contact surface preparations. The initial concept in the study is the six-probe method which was identified as the most practical to ensure a sufficient contact quality between specimen and probe. As mentioned before, the six-probe method does not require any surface pretreatment since the well-defined line contact in combination with the fabric's fibre bundles in the specimen's width direction are utilised to ensure the transverse homogeneity of the current distribution in the specimen's width direction. More importantly, one experiment determines both the in- and the out-of-plane electrical conductivity of polymer composites reinforced with carbon fabrics, simultaneously.

Theory

In this section, the six-probe measurement method is outlined followed by a numerical method to derive the anisotropic electrical conductivities from the measured voltages.

The six-probe voltage measurement method

In the six-probe method, an electrical current is applied at the top surface of a specimen over a distance L from point A to point B, as depicted in the two-dimensional schematic representation in Figure 3. As a result of the applied current between point A and B, a non-uniform electrical field density is generated in the specimen, shown by the dashed lines. The voltage drop measured over distance l at the top surface V_t is not equal to the measured voltage drop over the same distance l at the bottom surface V_b. The distribution depends on the distance L, the thickness of the specimen, and the in- and out-of-plane specific electrical conductivities of the specimen. For the herein presented method and the materials to be characterized, it can be assumed that the electrical current is evenly distributed over the width of a specimen due to the presence of the fabric's fibre bundles in this direction.

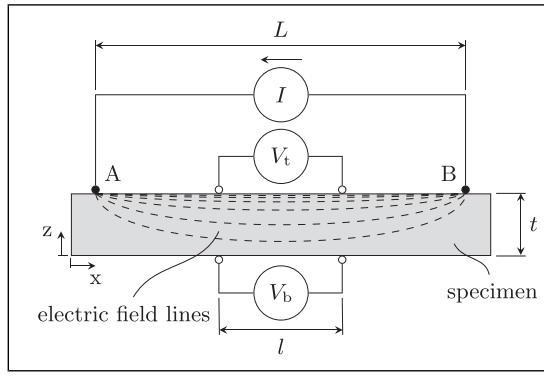

Figure 3. A cross-sectional view of a specimen undergoing a six-probe measurement.

Numerical model description

Hart and Zhupanska[33] developed a procedure to derive the anisotropic electrical conductivities from six-probe measurements on unidirectional composites. Their procedure expands upon work performed by Busch et al.,[36] in which an analytical approximation is presented to measure the electrical conductivity of strongly anisotropic single crystals using the six-probe method. This analytical approximation can be obtained by solving the differential equation describing the two-dimensional potential distribution $V(x, z)$ in the specimen during a six-probe experiment,

$$\frac{1}{\rho_x}\frac{d^2V}{dx^2}+\frac{1}{\rho_z}\frac{d^2V}{dz^2}=0. \tag{5}$$

An appropriate solution is given by expansion

$$V(x,z)=\sum_{n=1,3,5,\ldots} V_n \sin\left(\frac{n\pi x}{L}\right)\cosh\left(\sqrt{\frac{\rho_z}{\rho_x}}\,\frac{n\pi z}{L}\right), \tag{6}$$

in which ρ denotes the electrical resistivity, the reciprocal of σ. The x and z in the subscripts of ρ represent the direction of the considered resistivity, agreeing with the x- and z-directions depicted in Figure 3. Busch et al. approximated $V(x, z)$ by only considering the lowest $n = 1$ term and obtained:

$$V(x,z)\approx -\frac{I}{w}\sqrt{\rho_z\rho_x}\,\frac{\sin(\pi x/L)}{\sinh\left((\pi t/L)\sqrt{\rho_z\rho_x}\right)}\cosh\left(\frac{\pi z}{L}\sqrt{\frac{\rho_z}{\rho_x}}\right). \tag{7}$$

Using the measured voltages V_t and V_b at the known locations one obtains from the ratio V_t/V_b,

$$\sqrt{\frac{\rho_z}{\rho_x}} \approx \frac{L}{\pi t} \operatorname{arccosh}\left(\frac{V_t}{V_b}\right) \tag{8}$$

and from V_t,

$$\sqrt{\rho_z \rho_x} \approx \frac{V_t w}{2I \sin\left(\frac{\pi l}{2L}\right)} \tanh\left(\frac{\pi t}{L}\sqrt{\frac{\rho_z}{\rho_x}}\right). \tag{9}$$

Dividing the result of equation (9) by the result of equation (8) gives ρ_x; multiplication of the result of equation (9) by the result of equation (8) gives ρ_z.

If this approach were to be applied to characterise the electrical conductivities of a TPC, this would be limited to lay-ups in which all plies are oriented. To be able to measure the electrical conductivities of arbitrary lay-ups (e.g. quasi-isotropic) it was decided to develop a straightforward numerical approach in which more than one ply orientation in the lay-up can be analysed to derive the specific electrical conductivities from six-probe measurements. Our results include a comparison of the conductivity values obtained using the numerical approach with values obtained using Busch's method.

In the numerical model, the specimen is considered as a number of stacked plies in which each ply is regarded as a number of resistances in series, R_x, shown in Figure 3. The plies are electrically connected to each other by out-of-plane resistances, R_z. R_z represents all resistances in the through-thickness direction, thus intra ply, inter ply and the constituents. Consequently, a so-called resistor grid is created as schematically shown in Figure 4, in which Δx represents the distance between the nodes in x-direction and Δz the distance between the nodes in z-direction. The values of R_x and R_z are calculated according to

$$R_x = \frac{1}{\sigma_x}\frac{\Delta x}{w \Delta z}, \tag{10a}$$

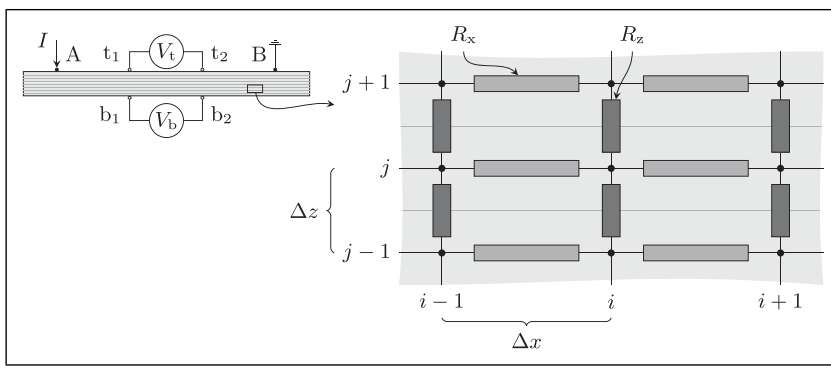

Figure 4. Schematic overview of the numerical representation of the electrical conductivity of a specimen.

$$R_z = \frac{1}{\sigma_z}\frac{\Delta z}{w\Delta x}, \tag{10b}$$

in which σ_x and σ_z are assumed to be uniform throughout the specimen.

A general nodal analysis is performed to compute the unknown voltages in this grid, after which the estimation of σ_x and σ_z is improved by means of minimizing the error between the measured voltages V_t and V_b, and the calculated voltages at the corresponding nodes in the grid. An extensive explanation of the general nodal analysis can be found in,[37] nevertheless a description is briefly summarised here for convenience together with the minimisation process.

To determine the unknown voltages, Kirchhoff's current law is combined with Ohm's law to formulate an objective function $\mathbf{F_1}$. Kirchhoff's current law[37] is described, in discrete form, by,

$$\mathbf{c} = \sum_{k=1}^{n} i_n, \tag{11}$$

in which i_n denotes the currents between the nodes in the grid and $\mathbf{c}$ represents the known sources. According to Kirchhoff's current law, these are zero at every node except at the nodes where it is fixed, corresponding to the positions A and B in Figure 4 between which I is applied to the specimen. Ohm's law, in turn, is described by

$$\mathbf{i} = \mathbf{G}\mathbf{v}, \tag{12}$$

where the currents in the grid are represented by $\mathbf{i}$. $\mathbf{G}$ is the matrix consisting of the discrete conductance values between the node points in the grid and $\mathbf{v}$ represents the nodal voltages. Subsequently, the objective function $\mathbf{F_1}$ is formulated according to

$$\mathbf{F_1} = |\mathbf{G}\mathbf{v} - \mathbf{c}|. \tag{13}$$

The unknown nodal voltages are obtained by minimising $\mathbf{F_1}$ using estimated initial values for σ_x and σ_z and starting with initial values for $\mathbf{v}$ within the expected range. To improve these estimated values for σ_x and σ_z, the calculated voltage drop between the nodes corresponding to t_1 and t_2 is compared with V_t and the voltage drop between the nodes corresponding to b_1 and b_2 is compared with V_b. The estimations of σ_x and σ_z are improved by minimising the difference between the measured voltages and the computed voltages, mathematically described by

$$\mathbf{F_2} = \min\left| \begin{Bmatrix} V_t \\ V_b \end{Bmatrix} - \begin{Bmatrix} |v_{t1} - v_{t2}| \\ |v_{b1} - v_{b2}| \end{Bmatrix} \right|, \tag{14}$$

in which $|v_{t1} - v_{t2}|$ and $|v_{b1} - v_{b2}|$ refer to the voltage drop between the nodes at position 1 and 2 at the top and bottom surface in Figure 4, respectively. A flowchart of the above described procedure is provided in Figure 5.

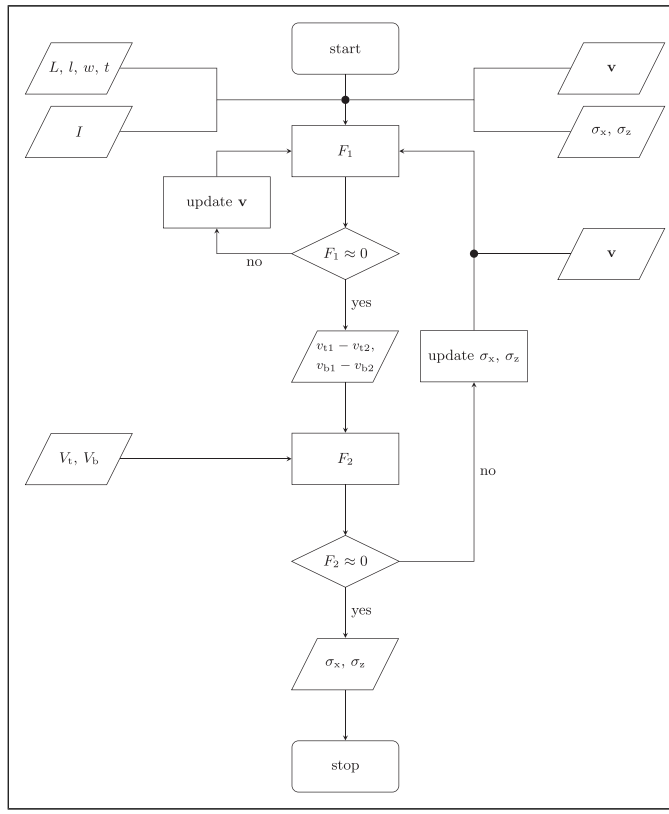

Figure 5. Flowchart of the numerical method to determine the anisotropic electrical conductivities from six-probe voltage measurements.

The objective functions $\mathbf{F_1}$ and $\mathbf{F_2}$ were minimised separately using a Levenberg-Marquardt least square method.[38]

Experimental work

A test program has been conducted to assess whether the six-probe method meets the objective of this study to have a simple and reliable measurement method to determine the anisotropic electrical conductivities of a carbon fabric reinforced TPC. The influence of the specimen width and thickness on the six-probe measurements was investigated. Other experiments were performed to investigate the effect of the distances between the probes. Finally, the numerical method to obtain the electrical conductivities was assessed, using the two-probe method to obtain a reference value for σ_z. The complete test matrix is presented in Table 2.

Table 2. Test matrix for experimental assessment of the six-probe method. The dimensions t, w, l and L are defined in Figure 3. The fibre volume content, φ_f, was 0.51 ± 0.01. Per configuration, six specimen were tested.

Set	Purpose	Method	Lay-up	t [mm]	w [mm]	l [mm]	L [mm]	Batch [#]
A	effect of w and t on σ	six-probe	$[(0,90)]_{2s}$	1.25 ± 0.00	10, 20, 30	40	120	1
			$[(0,90)]_{4s}$	2.47 ± 0.01				
			$[(0,90)]_{6s}$	3.73 ± 0.02				
B	effect of l and L on σ, constant l/L-ratio	six-probe	$[(0,90)]_{4s}$	2.47 ± 0.01	20	40	120	1
						50	150	
						60	180	
						70	210	
						80	240	
C	effect of l and L on σ, varying l/L-ratio	six-probe	$[(0,90)]_{4s}$	2.47 ± 0.01	20	40	240	1
						60		
						80		
						100		
						120		
						140		
						160		
D	validate num. method	six-probe	$[(0,90)]_{2s}$	1.25 ± 0.00	20	40	120	2
			$[(0,90)]_{4s}$	2.50 ± 0.01				
			$[(0,90)]_{6s}$	3.67 ± 0.01				
E	validate num. method	two-probe	$[(0,90)]_{2s}$	1.26 ± 0.01	15 × 15 mm^2			2
			$[(0,90)]_{4s}$	2.50 ± 0.01				
			$[(0,90)]_{6s}$	3.67 ± 0.02				

Materials

Carbon fibre reinforced polyphenylenesulphide (C/PPS) prepreg fabric material (Cetex® TC1100) from Toray Advanced Composites (Nijverdal, the Netherlands) was used in this work. The weave type of the balanced fabric is 5 harness satin (5HS). The prepreg details, as specified in the manufacturer's data sheet is presented in Table 3.

The laminates were consolidated using a picture frame mould of 305 × 305 mm^2 in a static press. The mould was heated at a rate of 10°C/min. To a temperature of 312°C, kept at this temperature for 10 min and subsequently cooled down to room temperature at a rate of 5°C/min. The laminates were consolidated at a pressure of 10 bar. The resulting fibre volume content of the C/PPS composite laminates amounted 0.51 ± 0.01, which was calculated according to.

$$\varphi_f = \frac{n_{ply} W_f}{\varrho_f t}, \tag{15}$$

where the number of plies, the fabric areal weight and the fibre material density are represented by n_{ply}, W_f and ϱ_f respectively. Finally, the laminates were cut into individual specimens by CNC contouring. The tested lay-ups are summarized in Table 2. The

Table 3. Properties of fibre, neat resin and woven fabric prepreg as specified in the manufacturer's data sheet.

Property	Value
Fibre type	T300JB carbon
Number of fibres per tow	3000
Tow cross sectional area	0.11 mm^2
Fibre density, ϱ_f	1760 kg/m^3
Fibre areal weight, W_f	281 g/m^2
Fibre resistivity, ρ_f	1.7 $m\Omega/cm$
Fibre content by volume, φ_f	0.51
Polymer resin	Polyphenylenesulphide, PPS
Matrix density, ϱ_m	1.35 g/cm^3
Matrix electrical conductivity, σ_m	Negligible compared to σ_f
Resin content by weight	0.43
Consolidated ply thickness	0.31 mm
Prepreg density	1550 kg/m^3
Prepreg weight per ply	496 g/m^2

averaged specimen thicknesses are provided in the Appendix. The thickness of an individual specimen was determined by averaging three thickness measurements along the specimen's length.

The six-probe measurement set-up

A fixture was developed to perform the six-probe experiments, which is shown in Figure 6. The fixture consists of a stainless steel (AISI 304L) base plate to which four clamps can be attached at defined positions. A schematic cross-sectional view of a clamp is shown in Figure 6(a). A line contact between the probes and the specimen was pursued to generate a 2-dimensional electrical field as assumed in Figure 3. This line contact also provides a high contact pressure to improve the contact between probe and specimen and accurate dimensions of L and l. The electrodes are copper plates with a designed knife edge with a slope angle of 45°, which have not been deburred in order to obtain the smallest possible tip radius (the obtained tip radius was 10–50 μm) to create a line contact over the complete width of a specimen. To electrically insulate the electrodes from the metal components which is also thermally resistant, micanite, supplied by Kuhne Industry (Nijkerk, the Netherlands) was chosen. Micanite is a commercially available plate material consisting of approx. 90% micapowder and 10% silicone or epoxy binder material. The guiding rods in Figure 6(b) provide for the vertical guidance of the upper half of the clamps enabling accurate and reproducible in-plane positioning.

The clamping force is provided by commercially available horizontal toggle clamps (Bessey STC-HH70) which are able to provide a clamping force up to 2500N, according the specifications. The adjustable force was set to the maximum which has not been measured separately. As the contact resistance at the measurement probes does not play a

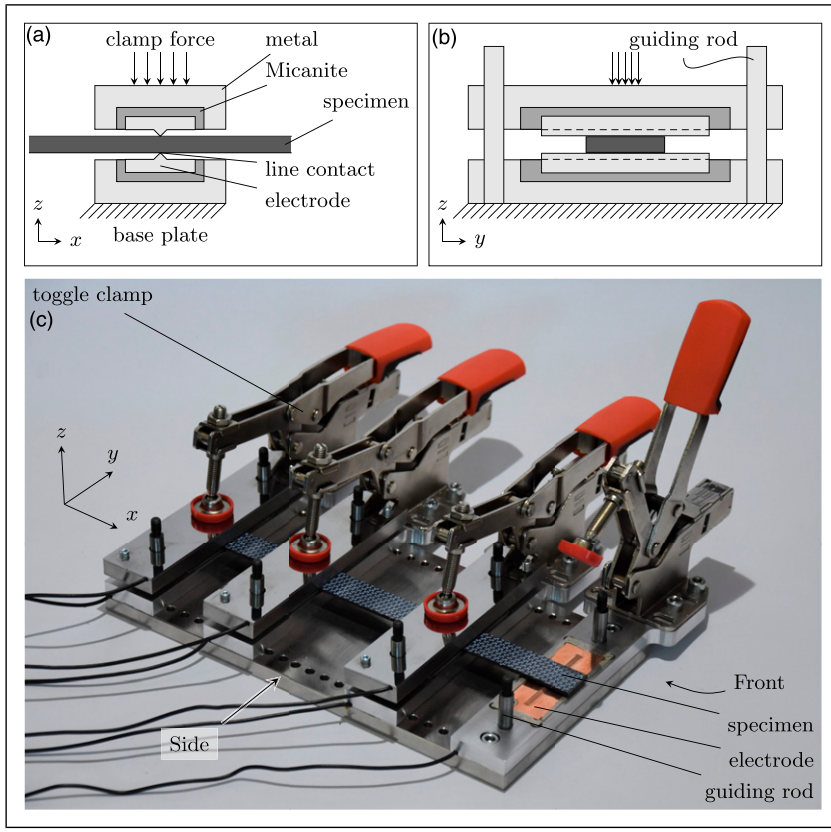

Figure 6. Overview of the six-probe test fixture, the cross-sectional views of one of the clamps shows the applied materials in the fixture; a) cross section side view; b) cross section front view; c) overall overview of the six-probe test set-up, depicted probe distances in the picture are L = 240 mm and l = 120 mm.

role in the six-probe measurements, it is assumed that this clamping force is sufficient to obtain consistent voltage measurements.

A direct current (DC) Lab power supply was used in combination with a TiePie HS6D-100 differential oscilloscope data acquisition system. Per experiment 5000 data points were generated over a time period of 50 ms at a sampling rate of 100 kHz. An electrical current of 200 ± 5 mA was applied in all six-probe experiments. The specimens did not show heating at this amperage, avoiding contingent thermal effects.

The two-probe measurement set-up

The validation of the σ_z values obtained by six-probe measurements consisted of a comparison with σ_z values retrieved from two-probe measurements. A DC Lab power

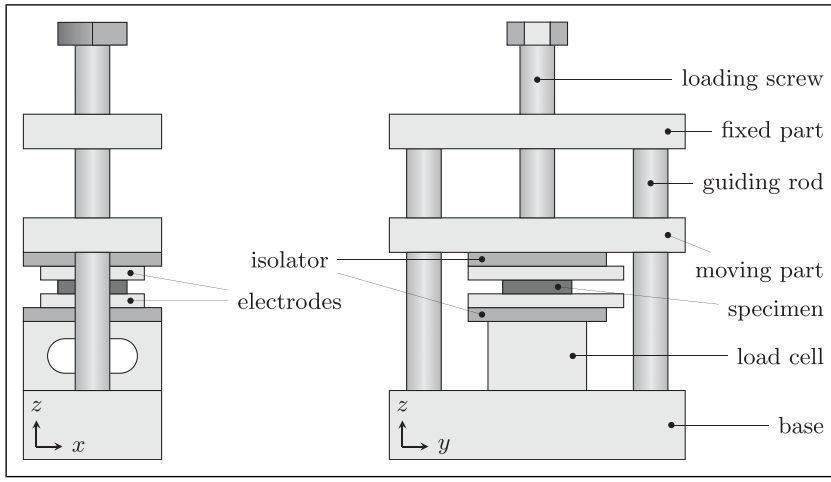

Figure 7. Schematic overview of the two-probe test fixture; (a) front view, (b) side view.

supply was used to apply a current, I, of 150 ± 5 mA to flat 25×25 mm^2 copper electrodes in between which a 15×15 mm^2 specimen was clamped with a force of $F = 1500 \pm 25$N. The clamp force was applied by a loading screw to a movable holder in which the upper electrode is placed. The guiding rods in Figure 7 provide for the vertical guidance of the upper electrode holder to ensure the in-plane positioning of the upper electrode. Electrically isolating material (Micanite) was placed between the electrode holders and the electrodes. The clamping force was measured using a load cell. An Arduino Uno was used to collect the data from the load cell and to measure the voltage drop. The specimens undergoing two-probe measurements required a surface pretreatment to ensure sufficient contact quality between electrode and specimen. The preparation of the specimen's contact surfaces consisted of machine polishing for 3 min with a Struers Tegramin 30 at a rotation speed of 80 rpm. and a force of 20 N. SiC Foil 2000 grit was used with water as coolant medium.

Experimental results

A typical six-probe test result is shown in Figure 8. The figure shows the voltage drop measured in an experiment where a 200 mA electrical current was applied to a 20 mm wide $[(0,90)]_{6s}$ specimen. The current was applied over a distance, L, of 240 mm and the distance, l, between the measurement probes was 160 mm. Both of the voltage drop measurements at the top and at the bottom surface of the specimen as well as their averages are represented, respectively 43.1 ± 5.9 mV and 20.8 ± 3.8 mV. The noise shown was considered acceptable and hence averaging the data points obtained during a measurement was applied as a data reduction method.

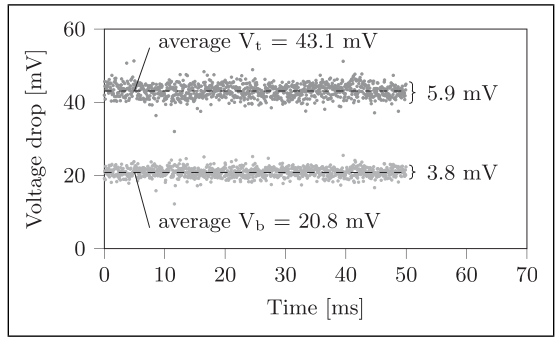

Figure 8. Typical test result of a $[(0,90)]_{6s}$ specimen; I = 200 mA, w = 20 mm, L = 240 mm, l = 160 mm, t = 2.47 mm.

Numerical model considerations. The distances between the nodes, explained in the numerical model description and shown in Figure 4, were determined based on a convergence study on a four ply specimen with the lowest value for L, 120 mm. The convergence study showed that 24 elements over L could sufficiently describe the gradient of the voltage potential between the current probes. Duplicating this amount to 48 elements did not provide a change larger than 1% of the electrical conductivities. Since homogenised σ_x and σ_z values are determined, Δz does not have to agree with the ply thickness, however the number of elements in thickness direction were set to agree with the number of plies in the laminate since the convergence study showed that decreasing Δz with a factor of 2 affected the electrical conductivity by 3%.

Results and discussion

The test data, provided in the appendix is discussed in this section for each investigated topic shown in Table 2. The graphs shown in this section present the mean values and the standard deviations provided in the tables in the appendix. Each mean value and standard deviation in the tables are obtained from experiments on six specimens.

The influence of the width and thickness of the specimen on the electrical conductivities

The voltages in the six-probe measurements of set A in Table 2 are presented in Figure 9. The specific data of these experiments is provided in Table A1 in the Appendix. Figure 9 shows low specimen to specimen variability and linearly increasing values of V with increasing values of $1/w$ as can be seen by the linear dashed lines provided as guide for the eye. The most apparent finding to emerge from the proportionality analysis is that the electrical current is properly distributed in the width direction at the positions of the voltage measurement probes. This justifies a 2-dimensional representation of the electrical

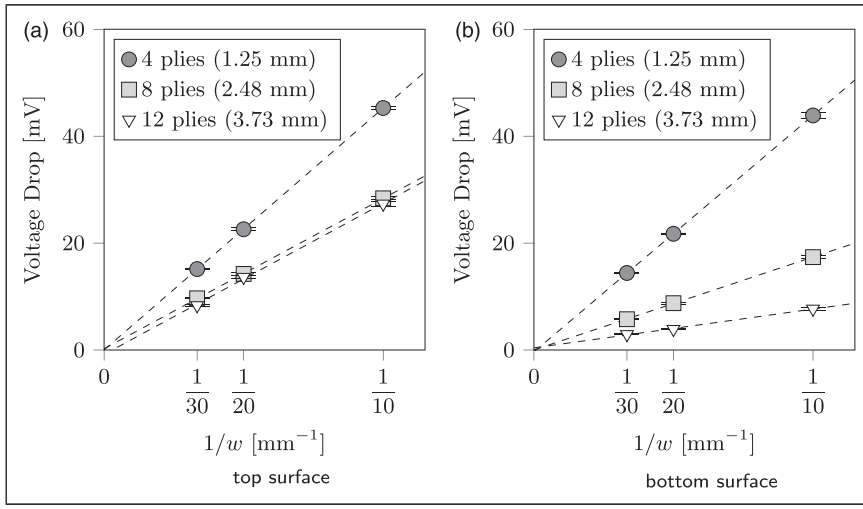

Figure 9. Overview of the voltage measurements in which the influence of *w* and *t* is investigated, set A in Table 2. (a) top surface, (b) bottom surface.

current distribution such as applied in the presented numerical method to derive the electrical conductivities from six-probe measurements in this case.

Figure 10 shows low specimen to specimen variability as well, however a non-linear relation between voltage drop and laminate thickness exists.

The voltages in the six-probe measurements were interpreted using the previously described numerical method to obtain the in-plane electrical conductivities, shown in Figure 11(a), and the out-of-plane electrical conductivities, shown in Figure 11(b). The σ_x values show high consistency independent of the number of plies in the laminate and the specimen width. This is in line with the expected electrical conductivity σ_x of 15.00 ± 0.29 kS/m, calculated using equation (2), and (15) and the data provided in Table 3. The σ_z values show less consistency, σ_z varies between 9.3 ± 0.3 and 19.0 ± 4.8 S/m. Moreover, for an increasing number of plies, a decrease of these values seems to be applicable which could indicate the existence of a thickness-related electrical resistance phenomenon, this can currently not be explained by e.g. differences in production since all laminates from which the specimens were taken underwent the same consolidation cycle. However, the obtained σ_z values in this set all fit within the characterised range obtained on a large proprietary dataset on the same material, this is represented by the gray area in the background of Figure 11(b), hence a thickness dependency cannot be concluded based on the limited amount of tested specimen in the present work.

The σ_z values, smaller by a factor of thousand than the σ_x values, also show a higher relative variability of 8.2% compared to the relative variability of 1.0% for the σ_x values. The relative variability increases with decreasing number of plies. The higher relative variability for the σ_z values could be explained by the specimen to specimen variation. The determination of σ_x is dominated by the V_t measurement, while the determination of

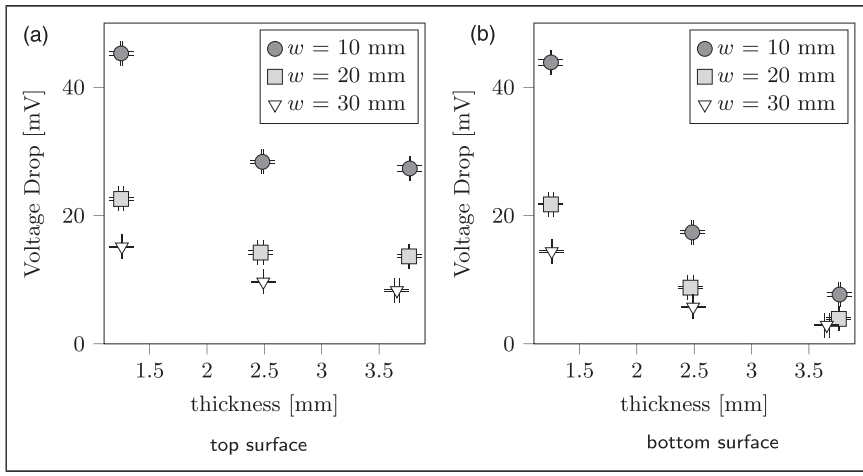

Figure 10. Overview of the voltage measurements of set A in which the influence of *w* and *t* is investigated. A non-linear relation between *V* and *t* is observed. (a) top surface, (b) bottom surface.

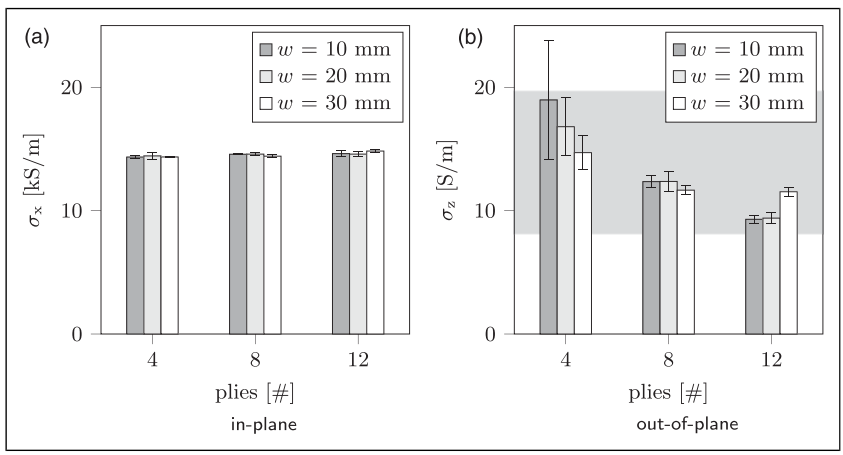

Figure 11. Overview of the electrical conductivities of set A in which the influence of *w* and *t* (represented in the Figure by the number of plies) is investigated. The gray area in the background of Fig. b represents proprietary conductivity data. (a) in-plane, (b) out-of-plane.

the σ_z value is dominated by the difference between V_t and V_b, while the absolute variability in $V_t - V_b$ remains similar to the absolute variability in V_t. This is visualized in Figure 12 where $V_t - V_b$ is shown alongside the V_t values of Figure 11(a), each on their own scale. This consideration shows that, in order to obtain low variability in the σ_z values, the width of a specimen should increase with decreasing thickness.

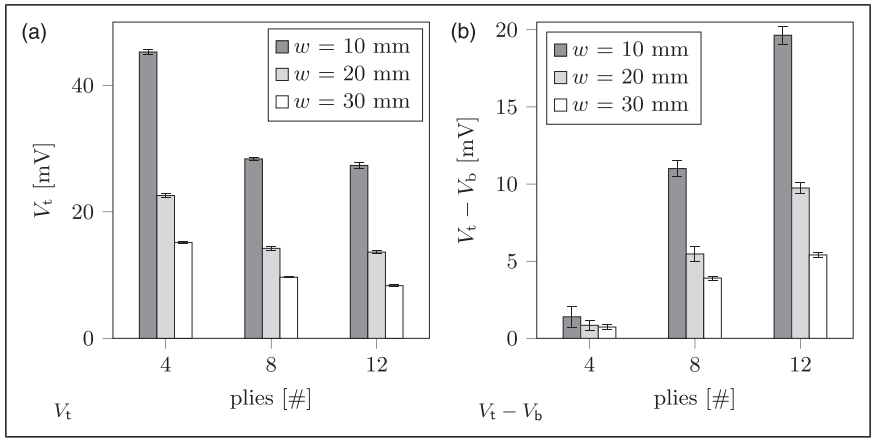

Figure 12. Representation of the voltage measurements to visualize the high relative variability in $V_t - V_b$ compared to the V_t measurements causing the high relative variablility in the σ_z values. (a) V_t, (b) V_t–V_b.

The influence of the probe distances on the electrical conductivities

The voltage measurements of set B and C are presented in Figure 13 for both the experiments with a constant L/l-ratio as well as the experiments in which l has been varied while L was kept constant at 240 mm. The voltage data shows low specimen to specimen variability.

The behaviour between probe distance and measured voltage depends on the l/L ratio. A small l/L ratio means that the measurement probes are not in the vicinity of the current introduction positions (points A and B in Figure 3), consequently the voltage measurements become less affected by the current introduction and shows a direct proportionality with the probe distance l. The opposite applies for a large l/L ratio, in that case the voltage measurements become affected by the current introduction and shows a higher order correlation with the probe distance. In Figure 13, second order polynomials are applied as visual guide for the regression lines, however it is more likely that a closed form description is more complex. The conductivity values of these experiments are provided in Tables A2 and A3 in the Appendix for the experiments with a constant L/l-ratio and for the experiments with a varying L/l-ratio, respectively. As can be observed from these experiments, the anisotropic electrical conductivities do not show significant dependency on the probe distance configurations tested.

Validation of the numerical method to determine the electrical conductivities from six-probe measurements

The electrical conductivities obtained from the six-probe voltage measurements in combination with the present numerical method is assessed in this section. The six-probe

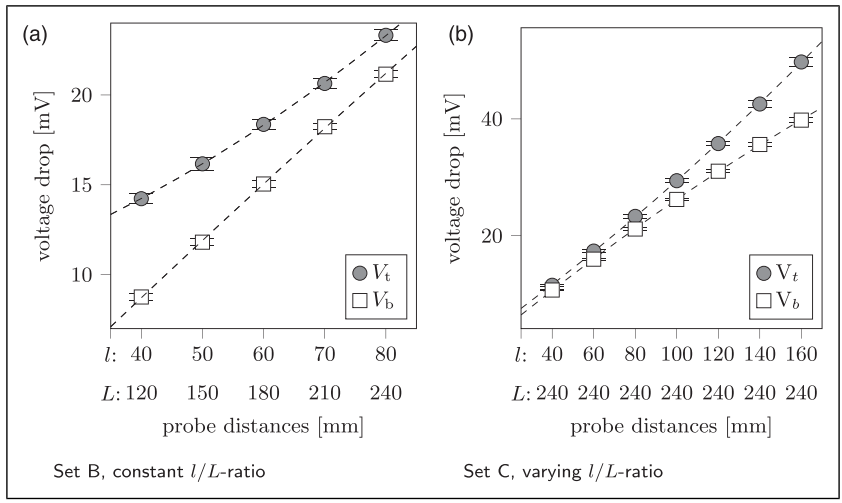

Figure 13. Overview of the voltage measurements to investigate the influence of *l* and *L*; second order polynomials were applied as a visual aid for the regression lines. (a) Set B, constant *l*/*L*-ratio, (b) Set C, varying *l*/*L*-ratio.

voltage data used in this section is provided in Table A4 in the Appendix alongside the numerically determined electrical conductivities. The two-probe data used in this section is provided in Table A5 in the Appendix.

The numerically determined σ_x values are compared with the σ_x values obtained, based on the same six-probe voltage data, using the analytical approach by Busch et al.,[36] equations (8) and (9), and with the calculated σ_x of 15.00 kS/m, previously obtained using the rule of mixtures.

The numerically determined σ_z values are compared with the σ_z values obtained using the analytical approach by Busch et al.[36] and with the σ_z values obtained from the two-probe measurements of set E. The two-probe data is presented in Figure 14 by means of the measured resistances, $R = V/I$. Figure 14 is depicted in terms of resistances since the intercept at $t = 0$ mm of 62 ± 23 mΩ, represents the average contact resistance between electrode and specimen. The average σ_z value was derived being 19.2 ± 0.7 S/m using the gradient $R/t = 231 \pm 9$ mΩ/mm and the specimen's cross-sectional area of 15×15 mm^2.

The anisotropic electrical conductivities obtained in experiment sets D and E, using all the different methods described above are presented in Figure 15. This overview shows high consistency in the σ_x values, regardless the applied analysis method. The overview of the σ_z values in Figure 15(b) does show a discrepancy between the approach by Busch et al. and the other two methods, especially for the 4-ply specimens. Due to the quite quickly converging σ_z values using Busch's method towards the σ_z values obtained using the other two methods for an increasing number of plies, it is presumed by the authors that the limited number of terms ($n = 1$) considered in equation (6) is inadequate for a sufficiently accurate description of the potential distribution $V(x, z)$ when the difference

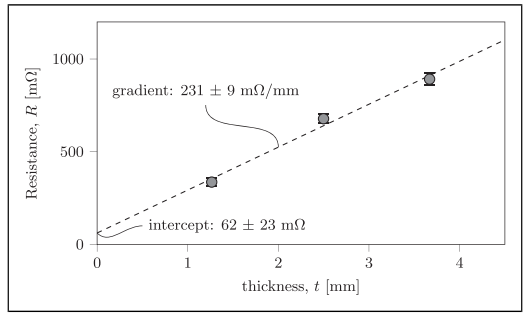

Figure 14. Overview of the two-probe voltage measurements of set E, performed to determine σ_z, to validate the numerical method.

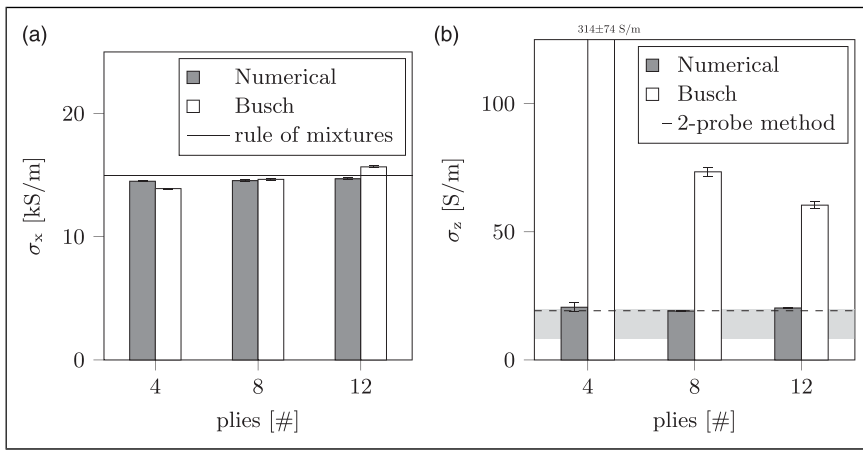

Figure 15. (a, b) Comparison of electrical conductivities obtained from two-probe and six-probe measurements in combination with the numerical method and the method proposed by Busch. The gray area in the background of Fig. b represents proprietary conductivity data.

between V_t and V_b is small, which is the case for low ply numbers. However, to check this assumption, complex mathematical derivations are needed (if even possible) which are beyond the scope of this work. The σ_z values obtained using the six-probe method in combination with the numerical method shows consistency with the σ_z values resulting from the two-probe measurements being 19.9 ± 1.2 S/m and 19.2 ± 2.0 S/m respectively.

As mentioned in the above, the intercept of 62 ± 23 mΩ at t = 0 mm in Figure 14 represents the average contact resistance between electrode and specimen. This immediately emphasizes two limitations of the two-probe method. Firstly, contact resistance is difficult to avoid, even after a meticulous surface pretreatment as described in section. Secondly, to obtain an estimate of the contact resistance it is inevitable to use multiple

specimens with different thicknesses. Based on the two-probe measurements on three different laminate thicknesses, only one average σ_z value was derived while the six-probe method does not require experiments on specimens with multiple thicknesses to characterise the anisotropic electrical conductivities.

A distinct difference in the σ_z values can be seen in Figure 11(b) compared to the σ_z values shown in Figure 15(b). In contrast to the σ_z values obtained in set A, shown in Figure 11(b), the σ_z values in Figure 15(b) does not show different σ_z values for the different specimen thicknesses. The obtained σ_z values in set D and E agree well with confidentially obtained σ_z values obtained from experiments on a large proprietary dataset which is shown by the gray area in the background of Figure 15(b). The limited amount of data in the present study is insufficient to make solid statements regarding thickness related phenomena affecting the out-of-plane electrical conductivity.

Conclusions

The overall objective of this study was to develop a simple and reliable method to measure the anisotropic electrical conductivity of a TPC material with a woven reinforcement. In this study, six-probe measurements were combined with a numerical approach to determine the anisotropic electrical conductivities. The study:

- demonstrates that a 2-dimensional representation of the electrical current distribution in the six-probe method is justified,
- shows that the present numerical method accurately calculates anisotropic electrical conductivities from six-probe measurements,
- validates the in-plane electrical conductivities obtained by six-probe measurements with in-plane electrical conductivities obtained by rule of mixtures,
- validates the out-of-plane electrical conductivities obtained by six-probe measurements with out-of-plane electrical conductivities obtained by two-probe measurements.

The conducted research shows that with one experiment, reliable in- and out-of-plane electrical conductivities of polymer composites reinforced with carbon fabrics can be determined simultaneously without the need of surface pretreatments. This represents an important simplification compared to other methods where the anisotropic electrical conductivities are determined with separate experiments and laborious surface pretreatments, required to ensure a proper introduction of the electrical current. The method can be applied to obtain the anisotropic electrical conductivity values required in induction heating simulations; another application beyond this paper is, for example, quality control of supplied materials.

Acknowledgements

The authors gratefully acknowledge the support from the industrial and academic members of the ThermoPlastic composites Research Center (TPRC), specifically the contribution from Toray

Advanced Composites regarding the proprietary dataset on the σ_z values and the work done by TPRC students S. Barts and N. Pizzigoni are greatly appreciated.

Declaration of conflicting interests

The author(s) declared no potential conflicts of interest with respect to the research, authorship, and/or publication of this article.

Funding

The author(s) disclosed receipt of the following financial support for the research, authorship, and/or publication of this article: This work was supported by the industrial and academic members of the TPRC.

ORCID iD


Sebastiaan van den Berg https://orcid.org/0000-0002-3633-7671

References

1. Airbus. *Global Market Forecast; Cities, Airports and Aircraft; 2019–2028*. AIRBUS SAS, Technical report, 2019.
2. Grand view research. *Carbon Thermoplastic (CFRTP) Composites Market Analysis By Raw Material (PAN, Pitch), By Application (Automotive, Aerospace and Defense, Wind Turbines, Sport, Construction Marine), and segment forecasts 2018–2025*. San Francisco, CA: Grand View Research, Inc, 2022.
3. Niu MCY. *Composite Airframe Structures*. (1st ed). Hong Kong: Conmilit Press Ltd, 1992.
4. Ageorges C, Ye L and Hou M. Advances in fusion bonding techniques for joining thermoplastic matrix composites: A review. *Compos. Part A Appl. Sci* 2001; 32(6): 839–857. DOI: 10.1016/S1359-835X(00)00166-4
5. Yousefpour A, Hojjati M and Immarigeon JP. Fusion bonding/welding of thermoplastic composites. *Journal of Thermoplastic Composite Materials* 2004; 17(4): 303–341. DOI: 10.1177/0892705704045187
6. Fink BK, Mccullough RL and Gillespie JW. A model to predict the planar electrical potential distribution in cross-ply carbon-fiber composites subjected to alternating magnetic fields. *Composites Science and Technology* 1993; 49: 71–80.
7. Kim HJ, Yarlagadda S, Gillespie JW, et al. A study on the induction heating of carbon fiber reinforced thermoplastic composites. *Advanced Composite Materials* 2002; 11(1): 71–80. DOI: 10.1163/156855102753613309
8. Miller AK, Chang C, Payne A, et al. The nature of induction heating in graphite-fiber, polymer-matrix composite material. *SAMPE Journal* 1990; 26(4): 37–54.
9. Rudolf R, Mitschang P and Neitzel M. Induction heating of continuous carbon-fibre-reinforced thermoplastics. *Compos. Part A Appl. Sci* 2000; 31(11): 1191–1202. DOI: 10.1016/S1359-835X(00)00094-4

10. Ahmed TJ, Stavrov D, Bersee HEN, et al. Induction welding of thermoplastic composites-an overview. *Compos. Part A Appl. Sci* 2006; 37(10): 1638–1651. DOI: 10.1016/j.compositesa.2005.10.009
11. Mitschang P, Rudolf R and Neitzel M. Continuous induction welding process , modelling and realisation. *J Thermoplast Compos Mater* 2002; 15: 127–153. DOI: 10.1106/089270502021451
12. Van Ingen JW, Buitenhuis A, Van Wijngaarden M, et al. Development of the gulfstream G650 induction welded thermoplastic elevators and rudder. In Sampe seattle 2010, p. 15.
13. COMSOL Inc. COMSOL multiphysics, 2019.
14. Dassault Systèmes. Abaqus FEA. 2019.
15. Bensaid S, Trichet D and Fouladgar J. 3-D simulation of induction heating of anisotropic composite materials. *IEEE Transactions on Magnetics* 2005; 41(5): 1568–1571. DOI: 10.1109/TMAG.2005.845047
16. Moser L. *Experimental Analysis and Modeling of Susceptorless Induction Welding of High Performance Thermoplastic Polymer Composites*. Technische Universität Kaiserslautern, 2012.
17. Pappadà S, Salomi A, Montanaro J, et al. Induction welding of pps-carbon composites: Modeling and experimental results. In: ICCM international conferences on composite materials, 2013 July, pp. 5481–5488.
18. Duhovic M, Moser L, Mitschang P, et al. Simulating the joining of composite materials by electromagnetic induction. *Simulating the Joining of Composite Materials by Electromagnetic Induction* 2014; 2: 1–22.
19. Lionetto F, Pappadà S, Buccoliero G, et al. Finite element modeling of continuous induction welding of thermoplastic matrix composites. *Mater Des* 2017; 120: 212–221. DOI: 10.1016/j.matdes.2017.02.024
20. Lundström F, Frogner K and Andersson M. Analysis of the temperature distribution in weave-based CFRP during induction heating using a simplified numerical model with a cross-ply representation. *Composites Part B: Engineering* 2021; 223: 223. DOI: 10.1016/j.compositesb.2021.109153
21. Hoffman T, Becker S, Duhovic M, et al. Simulating the induction heating behavior of CFRTPC laminates. In: *13th European LS-DYNA Conference*. Kaiserslautern: DYNAmore GmbH, p. 16.
22. Lundström F, Frogner K and Andersson M. A method for inductive measurement of equivalent electrical conductivity in thin non-consolidated multilayer carbon fibre fabrics. *Compos Part B: Eng* 2018; 140: 204–213. DOI: 10.1016/j.compositesb.2017.12.027
23. Lundström F, Frogner K and Andersson M. Numerical modelling of CFRP induction heating using temperature-dependent material properties. *Compos Part B: Eng* 2021; 220: 108982. DOI: 10.1016/j.compositesb.2021.108982
24. Mizukami K and Watanabe Y. A simple inverse analysis method for eddy current-based measurement of through-thickness conductivity of carbon fiber composites. *Polymer Testing* 2018; 69: 320–324. DOI: 10.1016/j.polymertesting.2018.05.043
25. Schulte K and Baron C. Load and failure analyses of CFRP laminates by means of electrical resistivity measurements. *Compos Sci Technol* 1989; 36(1): 63–76. DOI: 10.1016/0266-3538(89)90016-X

26. Todoroki A, Tanaka M and Shimamura Y. Measurement of orthotropic electric conductance of CFRP laminates and analysis of the effect on delamination monitoring with an electric resistance change method. *Compos Sci Technol* 2002; 62(5): 619–628. DOI: 10.1016/S0266-3538(02)00019-2
27. Gaier JR, YoderVandenberg Y, Berkebile S, et al. The electrical and thermal conductivity of woven pristine and intercalated graphite fiber-polymer composites. *Carbon* 2003; 41(12): 2187–2193. DOI: 10.1016/S0008-6223(03)00238-0
28. Todoroki A and Yoshida J. Electrical resistance change of unidirectional CFRP due to applied load. *JSME* 2004; 47(3): 357–364. DOI: 10.1299/jsmea.47.357
29. Lundström F, Frogner K and Andersson M. A numerical model to analyse the temperature distribution in cross-ply CFRP during induction heating. *Compos Part B: Eng* 2020; 202: 108419. DOI: 10.1016/j.compositesb.2020.108419
30. Wang S and Chung DDL. Electrical behavior of carbon fiber polymer-matrix composites in the through-thickness direction. *Journal of Materials Science* 2000; 35(1): 91–100. DOI: 10.1023/A:1004744600284
31. Guerrero VH and Chung DDL. Interlaminar interface relaxation upon heating carbon fiber thermoplastic-matrix composite, studied by contact electrical resistivity measurement. *Composite Interfaces* 2002; 9(6): 557–563. DOI: 10.1163/15685540260494128
32. Montgomery HC. Method for measuring electrical resistivity of anisotropic materials. *Journal of Applied Physics* 1971; 42(7): 2971–2975. DOI: 10.1063/1.1660656
33. Hart RJ and Zhupanska OI. The role of electrical anisotropy and effective conducting thickness in understanding and interpreting static resistance measurements in CFRP composite laminates. *Journal of Composite Materials* 2019: 1–16. DOI: 10.1177/0021998319870860
34. Mook G, Lange R and Koeser O. Non-destructive characterisation of carbon-fibre-reinforced plastics by means of eddy-currents. *Composites Science and Technology* 2001; 61(6): 865–873. DOI: 10.1016/S0266-3538(00)00164-0
35. Cheng J, Ji H, Qiu J, et al. Role of interlaminar interface on bulk conductivity and electrical anisotropy of CFRP laminates measured by eddy current method. *NDT and E International* 2014; 68: 1–12. DOI: 10.1016/j.ndteint.2014.07.001
36. Busch R, Ries G, Werthner H, et al. New aspects of the mixed state from six-terminal measurements on bi2sr2cacu20 single crystals. *Physical Review Letters* 1993; 69(3): 522–525.
37. Agarwal A and Lang J. Circuits and electronics. In: *Course materials for 6.002 Spring ed. chapter Basic Circ*. Massachusetts Institute of Technology, 2007, pp. 14–19.
38. Kelley C. *Iterative Methods for Optimization*. Philadelphia: Society for Industrial and Applied Mathematics, 1999.

Appendix

Table A1. Six-probe test results belonging to set A to investigate the influence of w and t on σ: I = 200 ± 5 mA, l = 40 mm, L = 120 mm.

		t [mm]		V_t [mV]		V_b [mV]		σ_x [kS/m]		σ_z [S/m]	
		Mean	std	Mean	std	Mean	std	Mean	std	Mean	std
Plies [#]	w [mm]										
4	10	1.25	0.01	45.3	0.3	43.9	0.5	14.3	0.1	19.0	4.8
	20	1.25	0.02	22.6	0.3	21.7	0.1	14.4	0.3	16.8	2.4
	30	1.26	0.00	15.1	0.1	14.4	0.1	14.4	0.1	14.7	1.4
8	10	2.48	0.01	28.4	0.3	17.4	0.2	14.6	0.0	12.3	0.5
	20	2.47	0.03	14.2	0.3	8.8	0.2	14.6	0.2	12.4	0.8
	30	2.49	0.00	9.7	0.1	5.8	0.1	14.4	0.1	11.7	0.4
12	10	3.77	0.01	27.3	0.5	7.7	0.2	14.6	0.2	9.3	0.3
	20	3.76	0.00	13.6	0.2	3.9	0.1	14.6	0.2	9.4	0.4
	30	3.66	0.02	8.3	0.1	2.9	0.1	14.8	0.1	11.5	0.4

Table A2. Six-probe test results belonging to set B to investigate the influence of l and L on σ with constant l/L-ratio: I = 200 ± 5 mA, w = 20 mm, l/L = 1/3.

		t [mm]		V_t [mV]		V_b [mV]		σ_x [kS/m]		σ_z [S/m]	
		Mean	std	Mean	std	Mean	std	Mean	std	Mean	std
l [mm]	L [mm]										
40	120	2.47	0.03	14.2	0.3	8.8	0.2	14.6	0.2	12.4	0.8
50	150	2.47	0.03	16.2	0.4	11.8	0.2	14.7	0.2	11.8	1.0
60	180	2.47	0.03	18.4	0.3	15.0	0.2	14.6	0.2	11.7	1.0
70	210	2.47	0.03	20.6	0.3	18.2	0.2	14.6	0.2	12.1	0.9
80	240	2.47	0.03	23.3	0.3	21.2	0.2	14.6	0.2	11.8	1.1
	Mean	2.47	0.03					14.6	0.2	12.0	1.0

Table A3. Six-probe test results belonging to set C to investigate the influence of l and L on σ with varying l/L-ratio on the electrical conductivity is investigated: I = 200 ± 5 mA, w = 20 mm.

		t [mm]		V_t [mV]		V_b [mV]		σ_x [kS/m]		σ_z [S/m]	
l [mm]	L [mm]	Mean	std	Mean	std	Mean	std	Mean	std	Mean	std
40	240	2.47	0.03	11.5	0.1	10.7	0.1	14.6	0.2	12.0	1.1
60	240	2.47	0.03	17.4	0.2	16.0	0.1	14.6	0.2	11.9	1.2
80	240	2.47	0.03	23.3	0.3	21.2	0.2	14.6	0.2	11.8	1.1
100	240	2.47	0.03	29.4	0.3	26.2	0.2	14.6	0.2	11.7	0.9
120	240	2.47	0.03	35.8	0.4	31.0	0.3	14.6	0.2	11.6	0.7
140	240	2.47	0.03	42.6	0.6	35.6	0.4	14.6	0.2	11.5	0.9
160	240	2.47	0.03	49.7	0.8	39.8	0.4	14.6	0.2	11.6	0.8
	Mean	2.47	0.03					14.6	0.2	11.7	0.9

Table A4. Six-probe test results belonging to set D to validate the numerical method: I = 200 ± 5 mA, w = 20 mm, l = 40 mm, L = 120 mm.

	t [mm]		V_t [mV]		V_b [mV]		σ_x [kS/m]		σ_z [S/m]	
plies [#]	Mean	std	Mean	std	Mean	std	Mean	std	Mean	std
4	1.25	0.00	22.3	0.1	21.7	0.1	14.5	0.0	20.6	1.8
8	2.50	0.01	13.2	0.1	9.1	0.1	14.6	0.1	19.1	0.3
12	3.67	0.01	11.3	0.1	4.6	0.0	14.7	0.1	20.3	0.4
mean							14.6	0.1	19.9	1.2

Table A5. Two-probe test results belonging to set E to obtain σ_z-values to validate the numerical method with: I = 150 ± 5 mA, $w \times l$ = 15 × 15 mm.

	t [mm]		F [N]		V [mV]		R [mΩ]	
plies [#]	Mean	std	Mean	std	Mean	std	Mean	std
4	1.26	0.01	1489	11	50.4	3.5	336	23
8	2.50	0.01	1507	24	101.7	3.8	678	25
12	3.67	0.02	1483	10	133.7	5.1	891	34